Journal of Volcanology and Geothermal Research 393 (2020) 106810

Contents lists available at ScienceDirect

Journal of Volcanology and Geothermal Research

journal homepage: www.elsevier.com/locate/jvolgeores

Variable mafic recharge across a caldera cycle at Rabaul, Papua New Guinea

Gareth N. Fabbro [a,*], Chris O. McKee [b], Mikhail E. Sindang [c], Stephen Eggins [d], Caroline Bouvet de Maisonneuve [a]

[a] Earth Observatory of Singapore, Nanyang Technological University, 50 Nanyang Avenue, 639798, Singapore
[b] Port Moresby Geophysical Observatory, PO Box 323, Port Moresby, NCD, Papua New Guinea
[c] Rabaul Volcano Observatory, PO Box 3386, Rabaul, Papua New Guinea
[d] Research School of Earth Sciences, Australian National University, Canberra, ACT 0200, Australia

ARTICLE INFO

Article history:
Received 14 August 2018
Received in revised form 28 January 2020
Accepted 3 February 2020
Available online 04 February 2020

Keywords:
Rabaul
Calderas
Magma mixing
Mafic recharge
Magma reservoirs

ABSTRACT

The size of eruptions from calderas varies greatly, from small effusive eruptions that pose danger only in the immediate vicinity of the vent, to large, caldera-forming events with global impact. However, we currently have little way of knowing the size of the next eruption. Here, we focus on Rabaul Caldera, Papua New Guinea, to investigate differences between the magmatic processes that occurred prior to the >11-km^3 caldera-forming "1400 BP" Rabaul Pyroclastics eruption and prior to subsequent, smaller (<1 km^3) post-caldera eruptions. During the current, post-caldera phase, basaltic enclaves and mafic minerals are common among the erupted products, indicating basalt has been free to enter the mobile, dacite-dominated region of the sub-caldera plumbing system. Many of the post-caldera magmas are hybrid andesites, reflecting the importance of mixing and mingling of basaltic and dacitic magmas during this period. In contrast, before the Rabaul Pyroclastics eruption, the recharge was an andesite that was not the product of mixing basalt and dacite. The lack of basaltic recharge prior to the Rabaul Pyroclastics eruption suggests basalt was prevented from entering the shallow, sub-caldera magma system at that time, possibly by the presence of a large, silicic, melt-dominated body. That basalt can currently enter the shallow system is consistent with reduced thermal and rheological contrasts between the recharge and resident magma, implying a similar large silicic melt body currently does not exist beneath the caldera. If this hypothesis is correct, it may be possible to track the growth and evolution of large magma reservoirs that feed caldera-forming eruptions by monitoring the petrology of eruptive products.

1. Introduction

While many caldera systems have repeated caldera-forming eruptions, their history is usually dominated by periods of smaller-scale activity and quiescence (e.g., Nairn et al., 1995; Druitt et al., 1999). There are always two questions about the next eruption—when, and how big? To answer the second question, understanding how magmatic systems evolve and behave prior to both small and large eruptions is needed. What causes a switch from frequent small eruptions to the discharge of a large volume of magma in one catastrophic event? Are there differences in the plumbing system prior to small and large events, and are there warning signals that could be detected?

The plumbing systems of long-lived volcanoes are complex, with regions of solidified plutonic material, partially solidified crystal mush, and crystal-poor melt (e.g., Cashman et al., 2017, and references therein), with only the crystal-poor parts being mobile and eruptible (Vigneresse et al., 1996; Dufek and Bachmann, 2010). As caldera-forming eruptions require a large, shallow reservoir of eruptible magma, tracking the formation of melt-dominated magma bodies can provide information about the potential size of the next eruption. We focus on Rabaul in Papua New Guinea, and in particular its most recent caldera-forming eruption. Intensive sampling has allowed us to determine the chemical and petrological stratigraphy of the deposits of this eruption in great detail, providing a snapshot of Rabaul's magma reservoir shortly before a caldera-forming eruption. This snapshot can be compared to what we know about the present-day plumbing system, gleaned from new petrological results as well as previous petrological and geophysical studies. By doing so, we reveal significant differences between the plumbing system prior to a large, caldera-forming eruption and the recent smaller eruptions.

2. Geological setting

Volcanism at Rabaul is related to the subduction of the Solomon Sea Plate below the South Bismarck Plate (Fig. 1; Johnson et al., 2010; Holm et al., 2016). The volcanism around Rabaul has been separated into three possibly connected systems (Johnson et al., 2010): a chain of mafic

* Corresponding author.
E-mail address: gareth.fabbro@cantab.net (G.N. Fabbro).

https://doi.org/10.1016/j.jvolgeores.2020.106810

stratovolcanoes (the Watom–Turagunan zone, WTZ), and two caldera systems, Tavui and the Rabaul Caldera Complex (RCC) on opposite sides of the WTZ (Fig. 1). The earliest dated volcanic deposits from the Rabaul area are lavas and scoria erupted from WTZ vents at about 500–300 ka (McKee and Duncan, 2016). Major explosive eruptions at the RCC started at about 200 ka, and include at least 10 dacitic ignimbrites, at least four of which are thought to have been erupted in the past ~20 ky (Nairn et al., 1995; McKee and Duncan, 2016).

2.1. The "1400 BP" Rabaul Pyroclastics

The most recent caldera-forming eruption took place between 667 and 699 CE (McKee et al., 2015), producing the "1400 BP" Rabaul Pyroclastics deposits—which comprise at least 11 km^3 of dacitic ash and pumice—and forming the latest caldera in Blanche Bay (Fig. 1; Heming and Carmichael, 1973; Walker et al., 1981). The deposits can be split into a fall component comprising a plinian unit and fine ash deposits and an overlying pyroclastic density current (PDC) deposit (Fig. 2; Heming, 1974; Walker et al., 1981). The fall deposits reach a maximum thickness of 1.31 m close to the caldera, and were distributed primarily to the southwest from a vent that was probably located in the center of what is now Blanche Bay (Walker et al., 1981). The fall deposits contain mainly coarse pumice clasts, overlying an ash deposit of up to 16 cm in thickness. Within the pumice fall deposit there are two or three prominent beds of fine ash that have a thickness of 4–5 cm over most of the dispersal area, and between the pumice fall and the PDC deposits there is also 35–40 cm of fine ash containing occasional accretionary lapilli (Walker et al., 1981). The PDC deposits vary systematically from 5 to 10 m in thickness near the caldera to about 0.5 m roughly 25 km from the caldera rim, and are referred to as "normal" ignimbrite (NI; Walker et al., 1981; Walker, 1983). Within paleo-valleys the PDC deposits can be much thicker—up to 30 m (Heming, 1974; Walker et al., 1981). The base of the PDC deposits is commonly weakly cross-bedded, suggesting formation by surges as the column began to collapse. These deposits are widespread and were interpreted as "ignimbrite veneer deposits" (IVD; Walker et al., 1981). Discontinuous, lithic-rich breccia layers occur at the base of the PDC deposit, and occasionally between two flow units within the PDC deposit. Walker et al. (1981) interpreted these as a ground layer deposited at the head of an advancing PDC. Another variant in the PDC deposits found close to the caldera is depleted in fine-grained clasts, and referred to as "fines-depleted ignimbrite" (FDI; Walker et al., 1981).

2.2. Post-Rabaul Pyroclastics activity

Following the Rabaul Pyroclastics caldera-forming eruption, volcanic activity became established at multiple vents spread across the caldera (Fig. 1). The youngest lava flow on Turagunan is stratigraphically younger than the Rabaul Pyroclastics caldera, and lava flows and pyroclastic deposits from Rabalanakaia, Tavurvur and Sulphur Creek have been dated at between about 770 and 175 years BP (Nairn et al., 1995; McKee et al., 2016).

Over the past 250 years (for which we have a relatively complete historical record) there have been at least nine eruptive episodes. The earliest recorded activity is the eruption of either Rabalanakaia or Tavurvur in 1767, mentioned by British explorer Philip Carteret (Hawkesworth et al., 1773, p. 596). Following this was the 1791 eruption of Tavurvur and the c. 1850 eruption of Sulphur Creek (Fig. 1; Fisher, 1939; Nairn et al., 1995; Johnson et al., 2010). Since then, eruptive activity has occurred at Vulcan and Tavurvur, two vents on opposite sides of the caldera (Fig. 1). Eruptive episodes in 1878, 1937–43 and 1994–2014 followed similar patterns (Fisher, 1939; Johnson et al., 1981; Johnson and Threlfall, 1985; McKee et al., 2018). Each commenced with strong explosive eruptions from both Vulcan and Tavurvur, followed by mainly vulcanian activity, which continued for months to years at Tavurvur.

The most recent period of activity started in 1994 (McKee et al., 2018) and was preceded by a period of major unrest between 1983 and 1985, with a large increase in seismicity and uplift of several metres centered on the caldera (McKee et al., 1989; Mori et al., 1989). In September 1994 Tavurvur started erupting, and within about 1 h Vulcan also reactivated. Vulcan's eruption column reached an estimated 18–30 km in height (Global Volcanism Program, 1994). Eruptions continued at Vulcan for fourteen days, and activity then continued intermittently at Tavurvur, predominantly in the form of weak to moderate vulcanian explosions or strong strombolian phases occasionally accompanied by lava flows. On 7 October 2006, Tavurvur experienced subplinian activity that sent an emission column 18 km high, to the base of the stratosphere (Global Volcanism Program, 2006). Intermittent activity continued until 29 August 2014, when strong strombolian activity from Tavurvur lasting several hours produced an emission column about 18 km in height (Global Volcanism Program, 2014). There have been no further eruptions since the August 2014 activity.

2.3. Geochemistry and petrology

Previous studies have shown that most volcanic rocks at Rabaul lie on a single liquid line of descent, termed the "main series" (Wood et al., 1995), with the exception of a few rhyolitic ignimbrites that are thought to have been erupted from the nearby Tavui caldera (McKee, 2015; Patia et al., 2017). Least-squares modelling shows that fractional crystallization can adequately explain most of this trend (Heming, 1974; Wood et al., 1995), although mixing of basalt and dacite is also required to explain some of the andesites (Patia, 2004; Bouvet de Maisonneuve et al., 2015; Patia et al., 2017).

3. Sample collection and analytical methods

88 samples of the Rabaul Pyroclastics deposits were collected from five locations, to sample the complete stratigraphy of the Rabaul Pyroclastics and to assess any lateral variation in the chemistry of this formation. Six further samples, representative of the complete sequence, were collected from Burma Road (Fig. 1) for detailed petrological analysis. Samples of the August 2014 eruption were collected by staff of the Rabaul Volcano Observatory 39 days after the eruption. Precise locations and sample descriptions are given in the Supplementary material.

Whole-rock chemical compositions were analyzed at the Research School of Earth Sciences, Australian National University and by Actlabs, Canada. Major elements were analyzed in minerals and glasses using a JEOL JXA-8530F electron microprobe at the Facility for Analysis Characterization Testing and Simulation, Nanyang Technological University, Singapore, using a 15 kV accelerating voltage and a 10 nA current. For mineral analyses a focused beam with a nominal diameter of 1 μm was used, and for glass analyses the beam was widened to 10 μm. Na and K were analyzed first to minimize the loss of alkalis. Counting times on peak positions were varied according to the element concentration: from 10 s for major elements and up to 100 s for trace elements (e.g., Mg in plagioclase). Backgrounds on both sides of the peak were measured for half of the peak time. ASTIMEX Mineral standards were used for calibration, and the relative error is <2% for major elements and 5–30% for minor and trace elements.

Melt inclusions were examined in BSE images, and the inclusions chosen for analysis were homogeneous and away from any cracks in the host crystal (Fig. 3a). The chemical similarity of the inclusions in the Rabaul Pyroclastics to whole-rock, matrix glass and inclusions in other units, along with the absence of bubbles and crystals visible in thin section, suggest that they have been subject to limited post-entrapment modification.

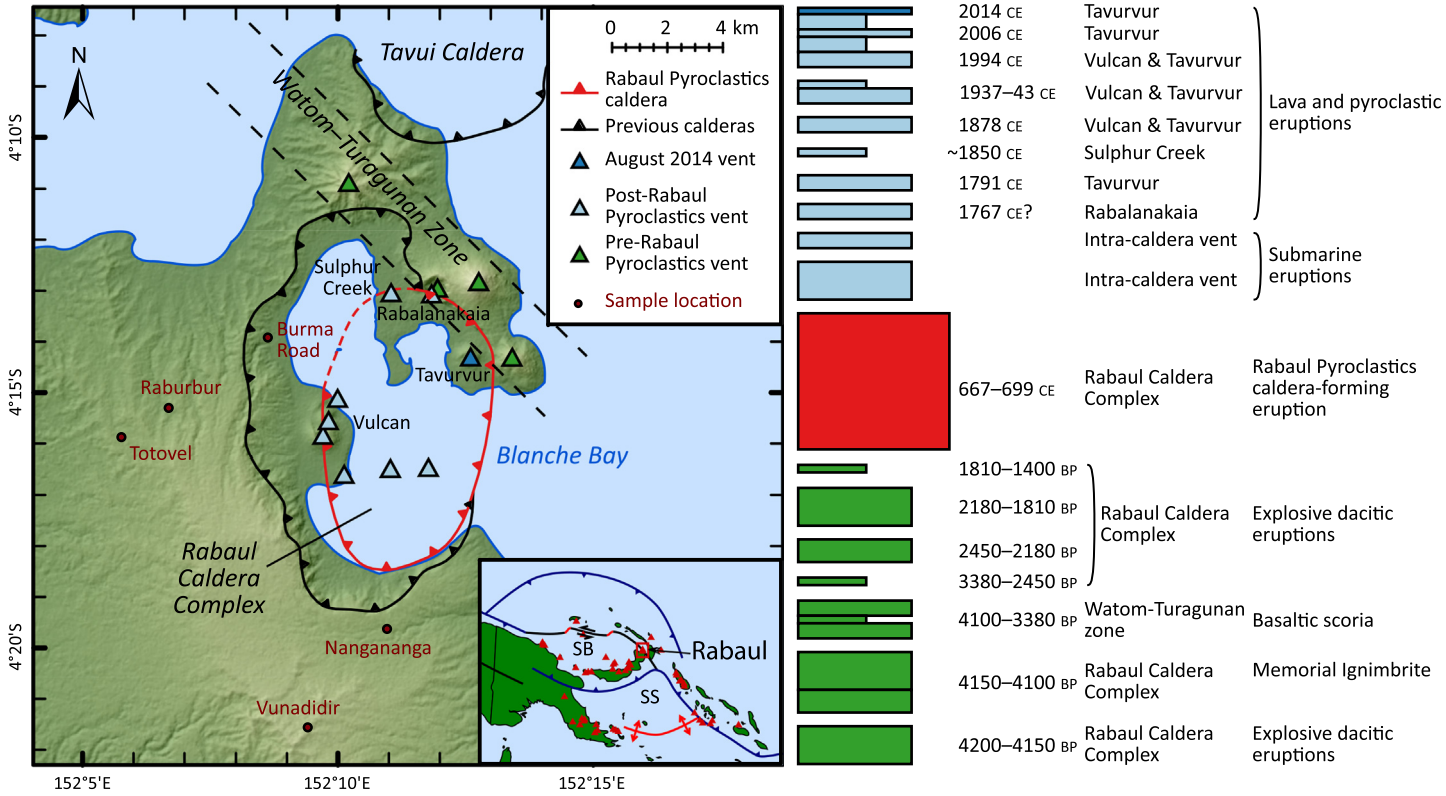

Fig. 1. Left: Map of the Rabaul Caldera Complex, adapted from Nairn et al. (1995). Inset: Location and tectonic setting of Rabaul. SB = South Bismarck Plate, SS = Solomon Sea Plate. Right: Schematic stratigraphic column showing simplified eruptive history of Rabaul since 4200 BP.

4. Results

4.1. The Rabaul Pyroclastics

The majority of the juvenile clasts in the Rabaul Pyroclastics are pale dacitic pumice that lie on the Rabaul "main series" chemical trend (Figs. 4–5; Wood et al., 1995). There is a slight zonation in the composition of these pumices with stratigraphic height (Fig. 2). The lowermost unit, the Basal Fine Ash, is the least evolved (64.4 wt% SiO_2), possibly due to juvenile material being mixed with fine lithic clasts. The overlying, coarser plinian deposits are more evolved (64.9–66.0 wt% SiO_2), and the Upper Fine Ash is more evolved again (66.3–66.6 wt% SiO_2). The Ignimbrite Veneer and Fines Depleted Ignimbrite deposits have similar chemistry to the Upper Fine Ash (65.1–66.5 wt% SiO_2), as does the base of the Normal Ignimbrite. There is then a trend towards less evolved compositions towards the top of the Normal Ignimbrite, down to 62.9 wt% SiO_2. Most of the matrix glass compositions from the pumice are tightly clustered between 67.5 and 68.6 wt% SiO_2. However, towards the top of the Normal Ignimbrite, there is a large spread, with some matrix glass having as little as 59.8 wt% SiO_2.

Darker pumice clasts are also present within the Rabaul Pyroclastics deposits. They tend to be less vesicular than the pale pumice, and the two varieties sometimes occur together as banded pumice. Compositions of the darker pumice range from 66.0 wt% SiO_2 (similar to the light pumice) down to 61.1 wt% SiO_2. Dense, glassy lithics similar in composition to the dark pumice are also found throughout the pyroclastic flow deposits.

The dacite is crystal-poor, with an average phenocryst content of 5.7 vol% comprising plagioclase (3.3 vol%), two pyroxenes (1.8 vol%), magnetite (0.5 vol%), and trace amounts of apatite. There is little variation in the composition of the phenocrysts with stratigraphic height through the Rabaul Pyroclastics (Fig. 2). Plagioclase rims are between An_{41} and An_{54} (Anorthite = 100 × molar Ca / [Ca + Na + K]), apart from a few calcic xenocrysts associated with mafic glass towards the top of the PDC deposits with rims of $An_{66–70}$ and cores of $An_{86–91}$. A small population of calcic plagioclase xenocrysts ($An_{85–95}$) was also reported by Patia (2004). Most plagioclase phenocrysts are either unzoned or have weak oscillatory zoning, and some have resorbed calcic cores (Fig. 3a, b). Pyroxene crystals are unzoned and have uniform compositions throughout the stratigraphy. Orthopyroxene crystals have compositions of $En_{69–72}Fs_{26–28}Wo_{2–4}$ and Mg# of 71–74 (Mg# = Mg number = 100 × molar Mg / [Fe + Mg]), and clinopyroxene crystals have compositions of $En_{44–46}Fs_{13–15}Wo_{39–42}$ and Mg# of 74–77. Melt inclusions in the phenocrysts have almost identical compositions to the dacitic matrix glass (68.0–70.2 wt% SiO_2).

4.2. August 2014 eruption

The magma erupted during the August 2014 eruption has a large compositional range, with SiO_2 varying between 56.7 and 63.4 wt%, similar to the entire compositional range of the post-1994 eruptions (Figs. 4–5; Patia, 2004; Bouvet de Maisonneuve et al., 2015). Plagioclase phenocrysts are either unzoned $An_{44–61}$, or have calcic cores of $An_{70–94}$

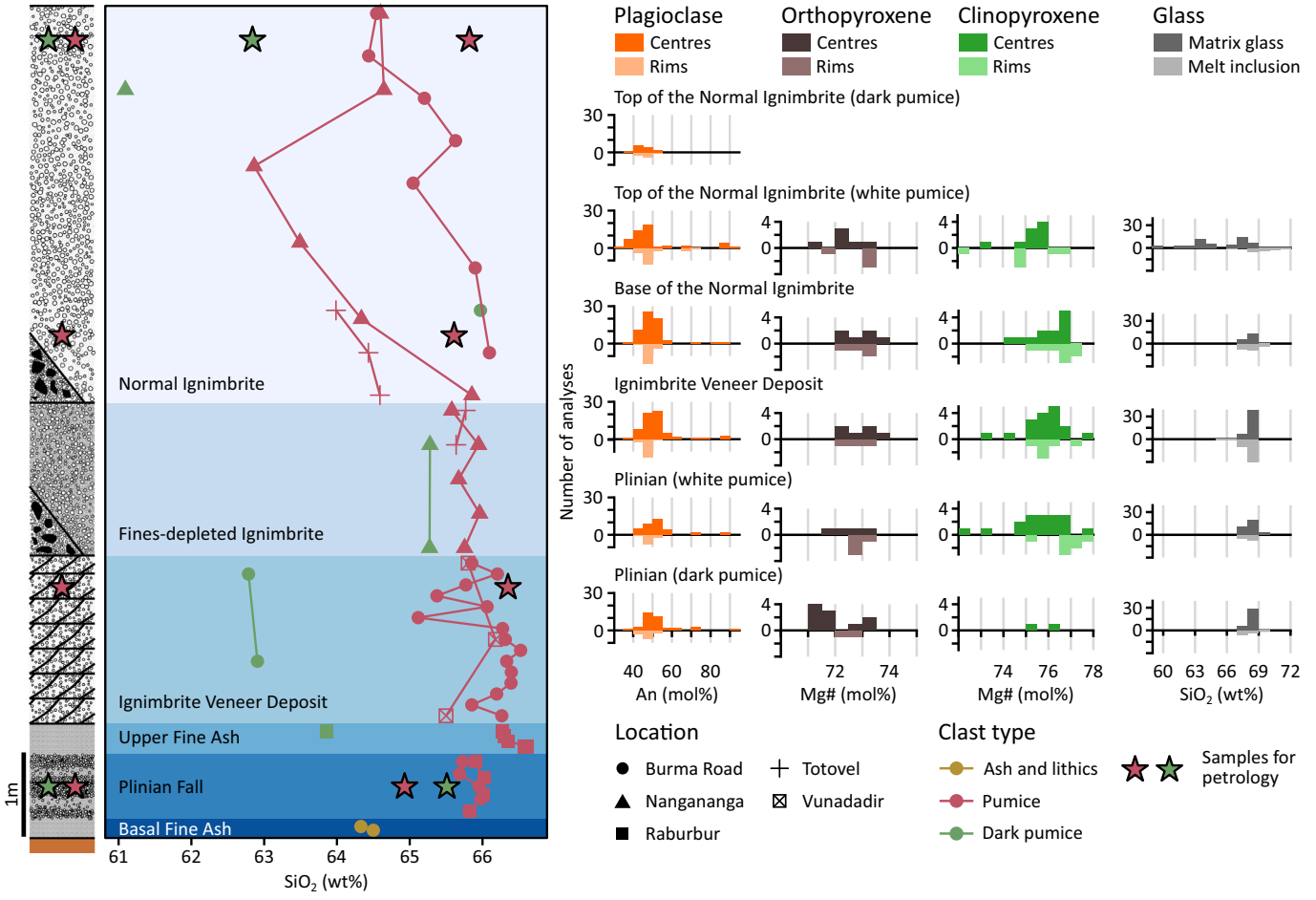

Fig. 2. Variations in the whole-rock, mineral, and glass chemistry of the Rabaul Pyroclastics with stratigraphic height. Synthetic stratigraphic column adapted from Walker et al. (1981). Red and green stars indicate the pale and dark pumice samples (respectively) used for the petrological work. Sample locations shown in Fig. 1. (For interpretation of the references to color in this figure legend, the reader is referred to the web version of this article.)

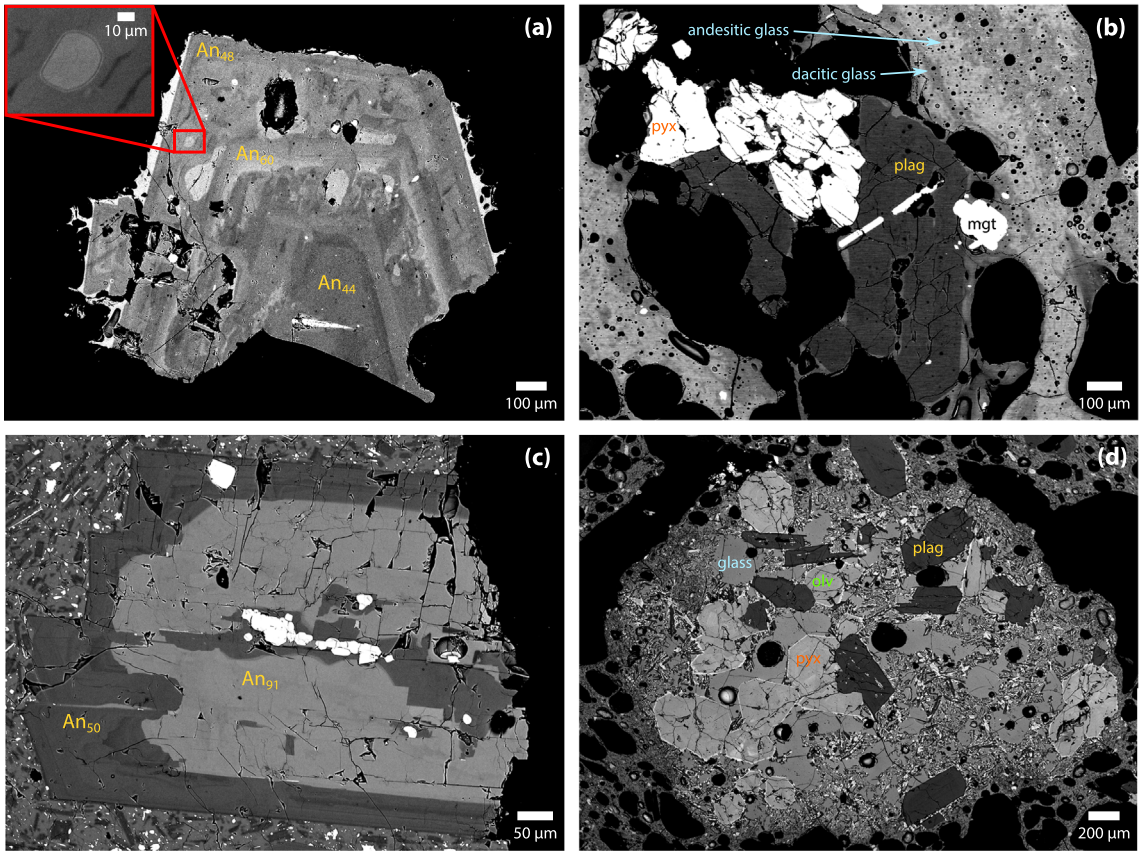

Fig. 3. BSE images of (a) a plagioclase crystal from the Rabaul Pyroclastics with melt inclusions, (b) mingled matrix glass from the top of the Normal Ignimbrite unit of the Rabaul Pyroclastics, (c) a zoned plagioclase crystal from the August 2014 eruption, and (d) a mafic enclave from the August 2014 eruption.

with rims of $An_{44–61}$ (Figs. 3c, 6). Orthopyroxene phenocrysts have compositions of $En_{70–74}Fs_{23–27}Wo_{2–5}$ (Mg# = 72–76), and clinopyroxene phenocrysts have compositions of $En_{39–46}Fs_{13–17}Wo_{39–46}$ (Mg# = 71–77). There is also a wide range in matrix glass compositions, with SiO_2 ranging from 62 to 68 wt% in the most mafic sample (RBL14-03) to 68–73 wt% in the most evolved (RBL14-02).

Mafic enclaves provide clear evidence for recharge shortly before eruption. These enclaves contain <1 mm crystals of unzoned calcic plagioclase ($An_{85–94}$), slightly more Mg-rich clinopyroxene ($En_{44–48}Fs_{7–12}Wo_{43–47}$; Mg# = 81–87), and olivine ($Fo_{73–83}$, Forsterite = 100 × molar Mg / [Mg + Fe]), all of which have 1–2 μm thick overgrowths of more evolved compositions (Fig. 3d). The groundmass of these enclaves contains symplectites of these three minerals, which along with the crystal overgrowths suggests rapid quenching.

4.3. Magma storage conditions at Rabaul

Magmatic temperatures were estimated using the plagioclase–liquid (Eq. (24a)), clinopyroxene–liquid (Eq. (33)), and two-pyroxene (Eq. (39)) thermometers of Putirka (2008). Valence states of Fe and Al in pyroxene were estimated using the algorithm of Papike et al. (1974). For plagioclase, only rim compositions were used in the calculations, as they best represent the conditions in the reservoir immediately prior to eruption. Clinopyroxenes and orthopyroxenes in this study are not strongly zoned, and using center or rim compositions produces similar temperatures and pressures.

The plagioclase–liquid and clinopyroxene–liquid thermometers require a pressure and water content as an input. We assumed a pressure of 1 kbar; changing the pressure from 0.5 to 2 kbar increases both the plagioclase–liquid and clinopyroxene–liquid temperature estimates by ~7 °C. The water content of the magmas is harder to pin down, and is discussed below.

4.3.1. Temperature

In the Rabaul Pyroclastics dacite, the plagioclase–liquid, clinopyroxene–liquid, and two-pyroxene thermometers of Putirka (2008) all give similar temperatures (Fig. 7). Assuming a melt H_2O content of 3 wt%, a pressure of 1 kbar, and using nearby matrix glass analyses as the liquid composition, plagioclase–liquid pairs give temperatures of 931–954 °C (mean = 941 °C; n = 37), clinopyroxene–liquid give 923–955 °C (mean = 943 °C; n = 5), and two-pyroxene touching pairs give 911–953 °C (mean = 931 °C; n = 16). One calcic plagioclase xenocryst surrounded by mafic melt gives a temperature of 1021 °C, and this most likely reflects the temperature of the andesitic recharge. An–Ab exchange coefficients suggest that the plagioclase rim compositions are in equilibrium with the matrix glass, and all of the plagioclase–liquid temperatures are lower than saturation temperatures (Eq. (24a)) with the exception of the calcic xenocryst that gives a temperature about 5 °C above the estimated saturation temperature. $K_D(Fe–Mg)^{cpx–liq}$ for the clinopyroxene crystals are within error of the expected values, and the temperatures they give are below the estimated clinopyroxene saturation temperatures (Eq. (34)). $K_D(Fe–Mg)^{cpx–opx}$ for the two-pyroxene pairs fall within the field of subsolidus equilibrium, possibly suggesting they were entrained from a mush zone in the reservoir, however they give similar temperatures to the plagioclase–liquid and clinopyroxene–liquid pairs.

The August 2014 eruption produced a wide range of whole-rock and matrix glass compositions, due to variable degrees of mixing and

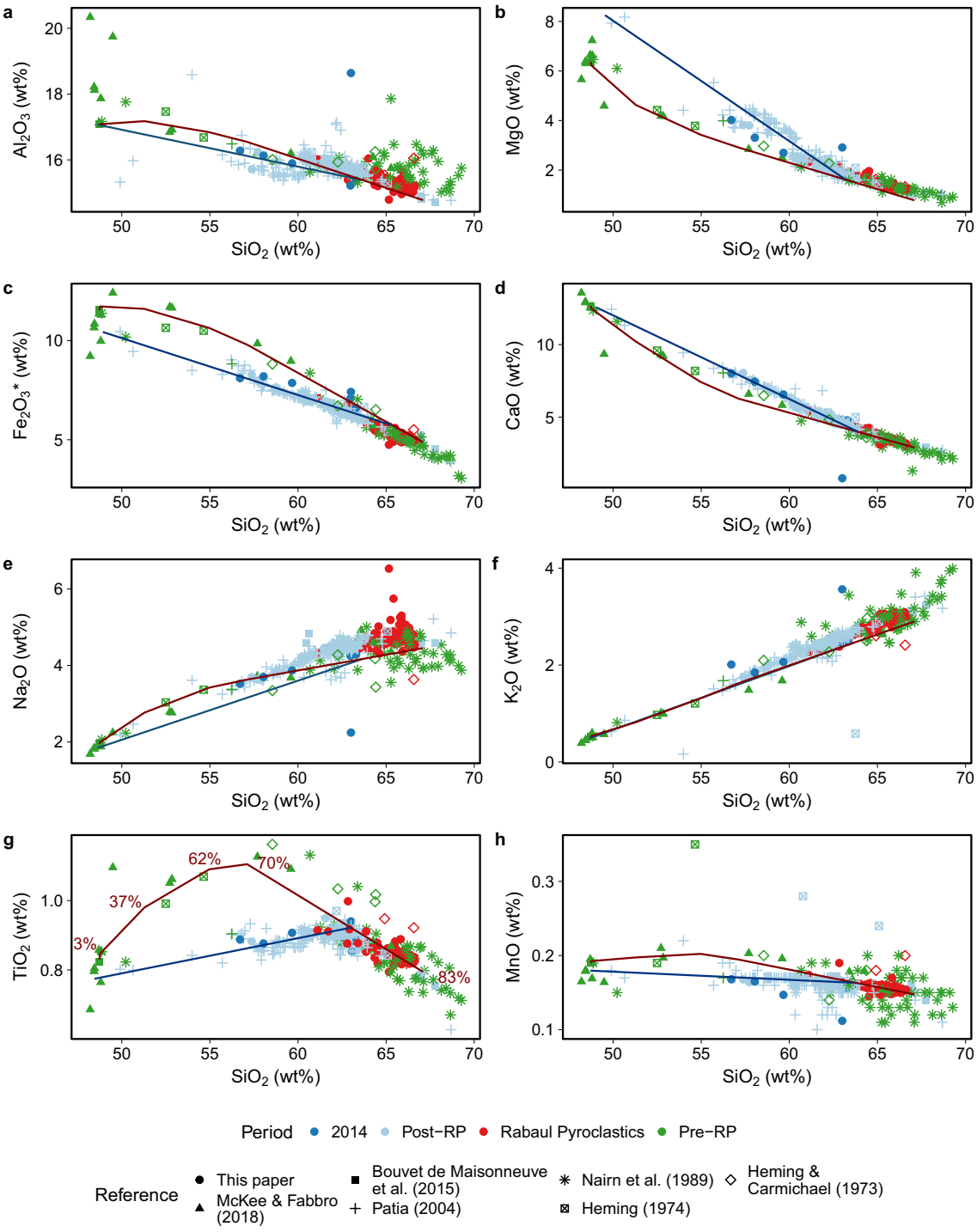

Fig. 4. Whole-rock major element variations of Rabaul magmas. Red line is the fractionation trend calculation discussed in Section 5.2, with the cumulative percentage of crystals removed shown in (g). Blue line is the mixing trend (McKee and Fabbro, 2018, Bouvet de Maisonneuve et al., 2015, Patia, 2004, Nairn et al., 1989, Heming, 1974 and Heming and Carmichael, 1973). (For interpretation of the references to color in this figure legend, the reader is referred to the web version of this article.)

groundmass crystallization. The pre-eruptive storage conditions of the August 2014 dacite are, therefore, best represented by the most evolved sample (RBL14-02). Neither the clinopyroxene nor the plagioclase crystals appear to be in equilibrium with the matrix glass, because the groundmass contains a large number of microlites and the matrix glass composition evolved in response to post- or syn-eruptive crystallization. Taking whole-rock compositions to represent the liquid, and assuming a melt H_2O content of 3 wt% and a pressure of 1 kbar, plagioclase–liquid pairs in RBL14-02 give temperatures of 974–1018 °C (mean = 989 °C; n = 28), and clinopyroxene–liquid pairs give 987–1001 °C (mean = 991 °C; n = 10). Only one non-xenocrystic two-pyroxene touching pair was analyzed, and this yielded a temperature of 943 °C. This two-pyroxene pair was found to have a similar $K_D(Fe–Mg)^{cpx–opx}$ to those in the Rabaul Pyroclastics. The plagioclase and clinopyroxene crystals found in the mafic enclaves appear to be in equilibrium with their matrix glasses, however plagioclase–liquid and clinopyroxene–liquid pairs in the enclaves give similar temperatures (plagioclase–liquid: 1000–1010 °C, mean = 1004 °C, n = 4;

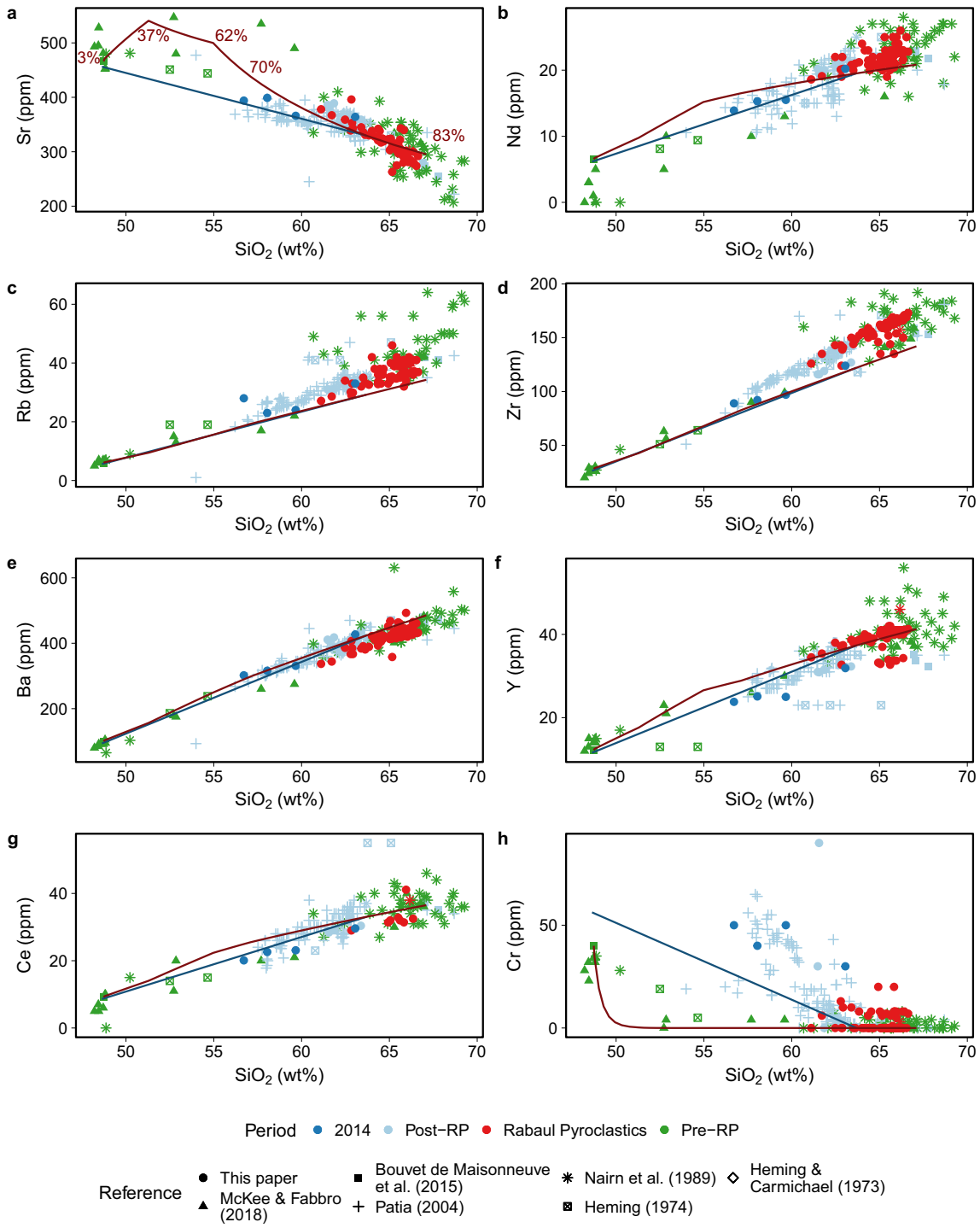

Fig. 5. Selected whole-rock trace element variations of Rabaul magmas. Red line is the fractionation trend calculation discussed in Section 5.2, with the cumulative percentage of crystals removed shown in (a). Blue line is the mixing trend (McKee and Fabbro, 2018, Bouvet de Maisonneuve et al., 2015, Patia, 2004, Nairn et al., 1989, Heming, 1974 and Heming and Carmichael, 1973). (For interpretation of the references to color in this figure legend, the reader is referred to the web version of this article.)

clinopyroxene–liquid: 966–1008 °C, mean = 986 °C, n = 12) to those in the dacite, suggesting that the crystals in the enclaves are recording the temperature after the mafic magma had been quenched by the dacite.

4.3.2. Pressure

The two-pyroxene barometer (Eq. (38) of Putirka, 2008) places the Rabaul Pyroclastics reservoir at between 2.0 and 5.1 kbar (mean = 3.6 kbar; n = 16). This is consistent with the one non-xenocrystic two-pyroxene pair analyzed from the August 2014 eruption (3.0 kbar), but below the maximum depth recorded by melt inclusion H_2O–CO_2 saturation pressures (closer to 1–2 kbar; Roggensack et al., 1996; Bouvet de Maisonneuve et al., 2015). The clinopyroxene–liquid pairs (Eq. (32c) of Putirka, 2008) in the Rabaul Pyroclastics give pressures that indicate a slightly shallower depth than that suggested by the two-pyroxene barometer (−0.9 to +2.7 kbar; mean = 0.9 kbar; n = 5), and that are consistent with the clinopyroxene–whole rock

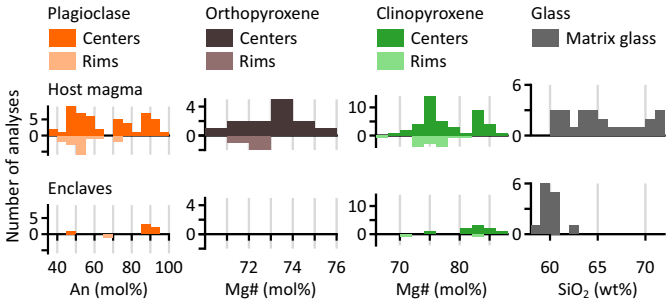

Fig. 6. Mineral and matrix glass chemistry of the August 2014 eruption.

pressures calculated for the August 2014 eruption (0.4–4.1 kbar; mean = 1.5 kbar; n = 10).

4.3.3. Water content

As we have no good independent estimate of the temperature, it is difficult to estimate the water content. Melt inclusions from the 1994 and 2006 eruptions contain 1–3 wt% H_2O (Roggensack et al., 1996; Bouvet de Maisonneuve et al., 2015), and plagioclase–liquid, clinopyroxene–liquid, and two-pyroxene pairs give similar temperatures if we assume a melt H_2O content of 3 wt%. Changing the assumed water content of the magma by 1 wt% changes our plagioclase–liquid temperatures by ~25 °C and our clinopyroxene–liquid temperatures by ~10 °C.

4.3.4. Summary

The Rabaul Pyroclastics dacite was probably stored at about 940 °C and 1–3 kbar, and the August 2014 dacite was probably stored at 990 °C and ~1.5 kbar, which is consistent with previous findings for other Rabaul eruptions.

5. Discussion

5.1. Generation of the Rabaul Pyroclastics dacite

The pre-Rabaul Pyroclastics deposits form a curved trend on plots such as TiO_2 against SiO_2 (Fig. 4g), suggesting compositional variability produced by fractional crystallization. We tested this hypothesis by modelling the trend, starting with the least evolved sample for which a comprehensive suite of major and trace element data was available (RBL12-24, a basalt from the WTZ; Bouvet de Maisonneuve et al., 2015). We used compositions of minerals from Rabaul taken from the data presented here and from previous studies (Heming, 1977; Patia, 2004; Bouvet de Maisonneuve et al., 2015). Major elements were modelled using mass balance calculations, and trace elements were modelled using the Rayleigh equation with partition coefficients taken from the GERM partition coefficient database (https://earthref.org/KDD/). The complete mineral compositions and partition coefficients used are available in the Supplementary material.

The following steps reproduce the data well, although our models slightly underestimate the concentrations of some incompatible elements such as K, Rb and Zr (Figs. 4–5):

1. 3% crystallization of An_{92} plagioclase (plag; 45%), Mg# 80 clinopyroxene (cpx; 45%), and Fo_{82} olivine (ol; 10%).
2. 35% crystallization of the residual liquid from step 1 of An_{92} plag (45%), Mg# 71 cpx (40.5%), Fo_{68} ol (10%), and magnetite (mag; 4.5%).
3. 40% crystallization of the residual liquid from step 2 of An_{72} plag (53%), Mg# 65 cpx (35%), Fo_{68} ol (5%), and mag (7%).
4. 20% crystallization of the residual liquid from step 3 with An_{62} plag (58%), Mg# 65 cpx (21%), Mg# 72 orthopyroxene (opx; 10%), and mag (10%).
5. 45% crystallization of the residual liquid from step four of An_{62} plag (60%), Mg# 65 cpx (10.8%), Mg# 72 opx (15%), mag (13%), and apatite (1.2%).

This indicates that up to 83% fractional crystallization, cumulatively, of similar basaltic parents is a viable process for generating the Rabaul Pyroclastics dacite and observed pre-Rabaul Pyroclastics magma compositions. Fractional crystallization could have been accompanied by crustal assimilation, but this is not required to explain Rabaul Pyroclastics compositions. We are unable to estimate to what degree assimilation may have occurred with the currently available data. As separating a melt from a crystal mush with >80% crystallinity is difficult (Vigneresse et al., 1996; Dufek and Bachmann, 2010), the Rabaul Pyroclastics dacite may have been generated in multiple stages of crystallization, melt differentiation, and segregation.

5.2. Changing mafic recharge across the caldera cycle

Quenched mafic enclaves are found in the deposits of the historical eruptions of Vulcan and Tavurvur, as well as the deposits from Rabalanakaia, although they have not been found in the deposits from Sulphur Creek (Patia, 2004; Bouvet de Maisonneuve et al., 2015; Patia et al., 2017). Some of the samples from 1937 and 1878 analyzed by

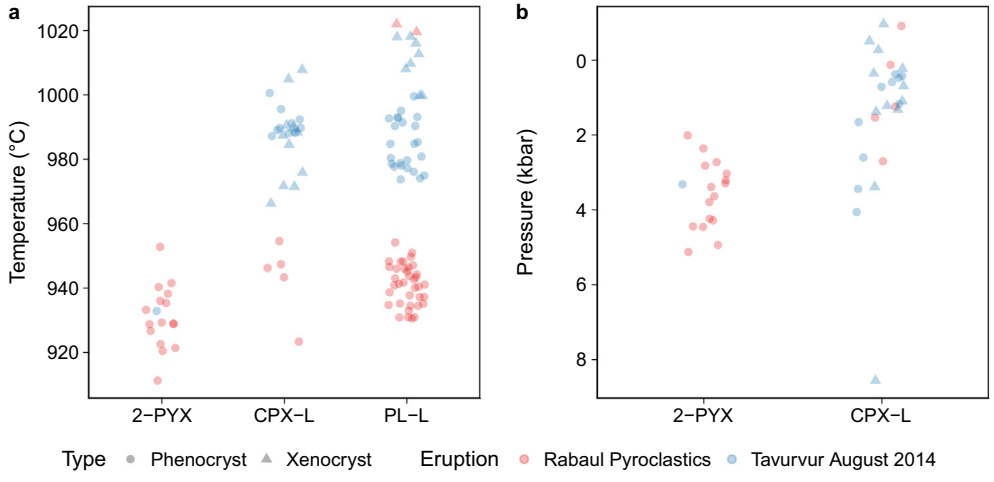

Fig. 7. Temperatures and pressures calculated using the two-pyroxene (2-PYX), clinopyroxene–liquid (CPX-L), and plagioclase–liquid (PL-L) thermometers and barometers of Putirka (2008), assuming a melt H_2O content of 3 wt%.

Patia (2004) are basaltic, and although most enclaves are too small to determine their whole-rock chemistry, their mineralogy is consistent with them being basaltic. The enclaves contain calcic plagioclase ($An_{85–97}$) and magnesian clinopyroxene (Mg# = 80–88), and olivine is present in enclaves in the deposit of the post-1994 eruptions and of some of the prehistoric eruptions of Tavurvur (Patia, 2004; Bouvet de Maisonneuve et al., 2015).

Plotting TiO_2 (and to a lesser extent MgO, Fe_2O_3*, CaO, MnO, Sr and Cr) against SiO_2 for the post-Rabaul Pyroclastics eruptives shows that many of these magmas are consistent with mixing of dacite with basalt (Figs. 4–5). Fractional crystallization forms curved trends on these plots, while the post-Rabaul Pyroclastics magmas form a straight line characteristic of mixing. The mixing trend for post-Rabaul Pyroclastics magmas intercepts the main fractionation trend at ~50 wt% SiO_2 on the mafic side, at compositions similar to the basaltic samples analyzed by Patia (2004) and slightly less evolved than the sample used to calculate fractional crystallization paths (RBL12-24). The mafic endmember of the mixing models shown in Figs. 4–5 was calculated by reversing step 1 of the fractional crystallization model and adding 7% crystals to RBL12-24. The silicic endmember is assumed to lie on the fractionation trend, with 63.8 wt% SiO_2. Because our fractional crystallization model slightly underestimates the concentration of some incompatible elements (such as K, Rb and Zr), our mixing model also slightly underestimates their concentrations.

The post-Rabaul Pyroclastics dacites plot on the silicic arm of the fractionation trend, and although most are less evolved than the Rabaul Pyroclastics dacite, there is some overlap. The whole array of post-Rabaul Pyroclastics magmas can be explained by mixing dacite formed through fractional crystallization with variable amounts of basalt. The mixing of basalt and dacite to form the magma erupted in 2014 can also be seen in the bimodal distribution of the compositions of the plagioclase and clinopyroxene centers in the host magma (Fig. 6). Xenocrystic cores match the composition of the crystals found in the enclaves.

The existence of quenched mafic enclaves suggests that mixing occurred only shortly before eruption. This is supported by both diffusion dating and $^{210}Pb/^{226}Ra$ activity ratio excesses in the post-1994 magmas. Plagioclase crystals that were transferred from a mafic magma to a more silicic magma prior to being erupted in the 2006 eruption could not have resided in the silicic magma for >2–3 decades, given their Sr and Mg profiles and the diffusivities of Sr and Mg in plagioclase (Bouvet de Maisonneuve et al., 2015). $^{210}Pb/^{226}Ra$ excesses in magmas erupted between 1994 and 1997 could be explained by gas transfer events within 1–10 years of eruption (Cunningham et al., 2009). Both of these estimates of the timescales of mafic recharge are consistent with basalt being injected into the dacitic reservoir sometime between the start of the 1983–1985 unrest up until the 2006 eruption started, possibly multiple times (Bouvet de Maisonneuve et al., 2015). An earlier phase of unrest started in 1971 (McKee et al., 1989; Johnson et al., 2010), and neither of the timescale estimates rules out the possibility of a phase of injection coinciding with this earlier unrest.

There is little zonation in either the dacitic component of the Rabaul Pyroclastics deposits or the phenocryst compositions. The decrease in the SiO_2 contents of the bulk composition of the pumice towards the top of the PDC deposits is likely due to the presence of more mingled mafic glass (Fig. 2). This suggests that the dacite was stored in a homogeneous, well mixed reservoir prior to eruption, which is consistent with the low crystallinity of the magma.

However, recharge also occurred shortly before the Rabaul Pyroclastics eruption, demonstrated by the dark pumice and andesitic glass found mingled in the deposits. The decrease in the SiO_2 content of erupted bulk compositions towards the top of the PDC deposit is consistent with the presence of more mingled mafic glass in these less evolved samples (Fig. 2). This recharge differs from that observed in the post-caldera magmas in two crucial respects: it is andesitic, and it is not associated with abundant mafic xenocrysts (Fig. 2). Furthermore, it plots along the fractionation trend, not the mixing trend of the Rabaul post-caldera magmas. Rather than being recharged by basalt—as is the case for the present-day shallow, dacitic reservoir—the Rabaul Pyroclastics reservoir was recharged by andesite (Fig. 8).

A change in recharge magma composition could be explained in two ways: (1) the composition of the primitive magma supplied from the mantle could have changed, becoming more mafic after the Rabaul Pyroclastics eruption, or (2) the composition of the primitive magma could have remained constant, but prior to the Rabaul Pyroclastics eruption this basaltic magma was unable to enter the shallow sub-caldera magma reservoir without first evolving to andesite. Given that the Rabaul Pyroclastics recharge magma composition plots along the fractionation trend for a large range of Rabaul products, it is more likely that mantle-derived basalt was unable to enter the shallow plumbing system prior to the Rabaul Pyroclastics eruption.

The closing-off of the shallow system to basalt has been demonstrated elsewhere. At Yellowstone, post-caldera basaltic eruptions have only occurred outside of the caldera margin, and this is attributed to a solidifying rhyolitic reservoir under the caldera (Christiansen, 2001; Christiansen et al., 2007). At Santorini, basalt was unable to reach the shallow system in the build-up to the 22-ka caldera-forming Cape Riva eruption (Fabbro et al., 2013). At Mt Mazama, Oregon, USA, the growing magma reservoir created a shadow zone, where regional basaltic magmatism was absent (Bacon and Lanphere, 2006; Karlstrom et al., 2015). At both of these volcanoes, a large stratocone was present, and the gravitational load imposed by the cone could have prevented the rise of basalt (Pinel and Jaupart, 2000). A large stratocone was not present at Rabaul prior to the Rabaul Pyroclastics eruption (Nairn et al.,

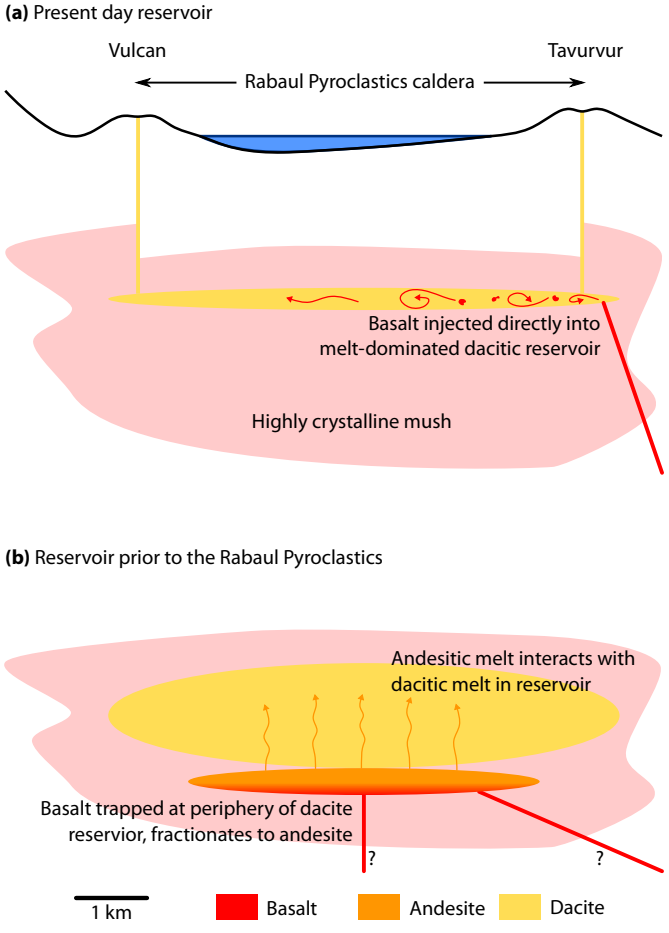

Fig. 8. Cartoon showing (a) the present day shallow reservoir under Rabaul and (b) the reservoir immediately prior to the Rabaul Pyroclastics eruption. Not vertically to scale.

1995). Stress changes due to reservoir overpressure can also prevent dykes from propagating to the surface through dyke capture (Karlstrom et al., 2015; Pansino and Taisne, 2019). However, dyke capture cannot explain why there was no interaction between basalt and dacite in the Rabaul Pyroclastics magma reservoir.

Differences in rheology make mixing of mafic and silicic magmas difficult as both magmas need to be sufficiently fluid at the same time to fully hybridize (Sparks and Marshall, 1986). If the mafic magma cools and crystallizes too much as it comes into contact with the silicic magma, it will become too viscous and be unable to mix. However, if the silicic magma body is relatively small, then this cooling will be limited, allowing mingling and hybridization to occur. Viscosities of the Rabaul basaltic recharge (initial composition used in step 1 of the fractional crystallization modelling, assuming 1 wt% H_2O, and T = 1180 °C), andesitic recharge (final composition of step 4, assuming 3 wt% H_2O and T = 970 °C), and resident dacite (final composition of step 5, assuming 5 wt% H_2O and T = 930 °C) are approximately 9 Pa·s, 850 Pa·s, and 2500 Pa·s, respectively, using the model of Giordano et al. (2008). The viscosity and temperature contrast are clearly much lower with an andesitic recharge (ratio of 3) than with a basaltic recharge (ratio of ~300), and therefore much more favourable to magma mixing, especially given that there is <30% mafic recharge involved (Sparks and Marshall, 1986).

The lack of basalt within the Rabaul Pyroclastics dacite thus suggests that prior to the Rabaul Pyroclastics eruption a dacitic melt-dominated body existed beneath Rabaul that was large enough to prevent the basalt from reaching the mobile part of the magma reservoir. Basalt supplied from depth would have been trapped at the periphery of this reservoir and would begin to crystallize, driving the residual liquid towards andesitic compositions. This andesite would have had less of a thermal and rheological contrast with the eruptible dacite, and would have been able to mix in small amounts with the dacite (Fig. 7). The andesite must have segregated from its crystals, to be consistent with the relative paucity of mafic crystals in the Rabaul Pyroclastics deposits. The reservoir that fed the climactic eruption of Mt Mazama was also recharged by an andesitic liquid (Bacon and Druitt, 1988), suggesting that this mechanism may not be unique to Rabaul. The draining of the eruptible part of the shallow reservoir during the Rabaul Pyroclastics eruption then allowed basalt to reach the shallow system, forming quenched basaltic enclaves in the post-Rabaul Pyroclastics dacites, a process noted at other caldera systems (Bachmann et al., 2012; Shane, 2015).

5.3. Construction of the caldera-forming magma reservoir

Recent work has suggested that crystal poor, caldera-forming magma bodies are ephemeral features in the shallow crust (e.g., Finney et al., 2008; Druitt et al., 2012; Allan et al., 2013; Fabbro et al., 2013, 2017; Cooper et al., 2017), and are assembled over the decades to centuries prior to eruption. The data we present here cannot provide any constraint on how long the Rabaul Pyroclastics reservoir resided in the shallow crust prior to the Rabaul Pyroclastics eruption. A high-Ti fractionated andesite, similar in composition to that found in the Rabaul Pyroclastics, is found as dark scoria in the predominantly dacitic, ~4.1-ka Memorial Ignimbrite of the Talili Pyroclastics period (McKee and Fabbro, 2018), suggesting that a large silicic reservoir was present at this time. Immediately above the Memorial Ignimbrite deposits lie three basaltic scoria deposits (Fig. 1), demonstrating that basalt could make it to the surface shortly after the discharge of this ignimbrite. This could represent an earlier cycle of the growth of a reservoir followed by its emptying, although the basaltic scoria were probably erupted from vents just outside of the caldera, in the WTZ (Fig. 1; Nairn et al., 1995; McKee and Fabbro, 2018) and therefore could have bypassed a large silicic reservoir present under the RCC. The RCC continued to erupt dacite, albeit of a slightly different composition to the Rabaul Pyroclastics (Nairn et al., 1995; McKee and Fabbro, 2018). The presence of basalt in the most recent eruptions, however, suggests that a single silicic melt body large enough to impede mantle-derived basalt is not currently present under Rabaul.

6. Conclusions

Detailed study of the Rabaul Pyroclastics shows that the progressive growth of a magma reservoir until it contains a large enough volume of mobile magma to generate a caldera-forming eruption is accompanied by a change in the composition of the recharge magma. Prior to a caldera-forming eruption, more primitive basaltic magma derived from depth is trapped at the periphery of the large reservoir and fractionates to andesite before it can mingle or mix with the resident dacite. Conversely, prior to a smaller scale intra-caldera eruption like the 2014 strombolian eruption of Tavurvur, mantle-derived basalt interacts directly with the resident dacite contained in a diminished reservoir. The differences in the plumbing system prior to small and large events at Rabaul are thus recorded in the eruptive products and can be recognized with detailed petrological investigations. Given the presence of basaltic magma mingled in the recent eruptive products, the current dacitic reservoir beneath Blanche Bay is probably reduced in size relative to that which existed prior to the Rabaul Pyroclastics eruption, and is unlikely to produce a caldera-forming eruption in the near future.

CRediT authorship contribution statement

Gareth N. Fabbro: Conceptualization, Methodology, Investigation, Data curation, Visualization, Writing - original draft. **Chris O. McKee:** Conceptualization, Investigation, Writing - review & editing. **Mikhail E. Sindang:** Investigation, Writing - review & editing. **Stephen Eggins:** Conceptualization, Resources, Investigation, Writing - review & editing. **Caroline Bouvet de Maisonneuve:** Conceptualization, Methodology, Investigation, Writing - review & editing, Supervision, Project administration, Funding acquisition.

Declaration of competing interest

The authors declare that they have no known competing financial interests or personal relationships that could have appeared to influence the work reported in this paper.

Acknowledgments

The authors wish to acknowledge the contribution of (late) Herman Patia to this paper for assisting with sample collection. This work was supported by the National Research Foundation Singapore and the Ministry of Education - Singapore under the Research Centres of Excellence initiative (Earth Observatory of Singapore contribution no. 280) as well as the Ministry of Education - Singapore Academic Research Fund Tier 1 RG178/16. COM and MES publish with the permission of the Secretary, Mr. Harry Kore, Department of Mineral Policy & Geohazards Management, Papua New Guinea. Resources for whole-rock geochemical analyses provided by the Research School of Earth Sciences, Australian National University.

Appendix A. Supplementary data

Supplementary data to this article can be found online at https://doi.org/10.1016/j.jvolgeores.2020.106810.

References

Allan, A.S.R., Morgan, D.J., Wilson, C.J.N., Millet, M.-A., 2013. From mush to eruption in centuries: assembly of the super-sized Oruanui magma body. Contrib. Mineral. Petrol. 166, 143–164. https://doi.org/10.1007/s00410-013-0869-2.

Bachmann, O., Deering, C.D., Ruprecht, J.S., Huber, C., Skopelitis, A., Schnyder, C., 2012. Evolution of silicic magmas in the Kos–Nisyros volcanic center, Greece: a petrological cycle associated with caldera collapse. Contrib. Mineral. Petrol. 163, 151–166. https://doi.org/10.1007/s00410-011-0663-y.

Bacon, C.R., Druitt, T.H., 1988. Compositional evolution of the zoned calcalkaline magma chamber of Mount Mazama, Crater Lake, Oregon. Contrib. Mineral. Petrol. 98, 224–256. https://doi.org/10.1007/BF00402114.

Bacon, C.R., Lanphere, M.A., 2006. Eruptive history and geochronology of Mount Mazama and the Crater Lake region, Oregon. Geol. Soc. Am. Bull. 118, 1331–1359. https://doi.org/10.1130/B25906.1.

Bouvet de Maisonneuve, C., Costa, F., Patia, H., Huber, C., 2015. Mafic magma replenishment, unrest and eruption in a caldera setting: insights from the 2006 eruption of Rabaul (Papua New Guinea). Geol. Soc. Lond., Spec. Publ. 422. https://doi.org/10.1144/SP422.2.

Cashman, K.V., Sparks, R.S.J., Blundy, J.D., 2017. Vertically extensive and unstable magmatic systems: a unified view of igneous processes. Science 355, eaag3055. https://doi.org/10.1126/science.aag3055.

Christiansen, R.L., 2001. The Quaternary and Pliocene Yellowstone Plateau Volcanic Field of Wyoming, Idaho, and Montana. U.S. Geological Survey Professional Paper. U.S. Geological Survey, Reston, Virginia.

Christiansen, R.L., Lowenstern, J.B., Smith, R.B., Heasler, H., Morgan, L.A., Mastin, L.G., Muffler, L.J.P., Robinson, J.E., 2007. Preliminary Assessment of Volcanic and Hydrothermal Hazards in Yellowstone National Park and Vicinity (Open File Report No. 2007–1071). U.S. Geological Survey, Reston, Virginia.

Cooper, G.F., Morgan, D.J., Wilson, C.J.N., 2017. Rapid assembly and rejuvenation of a large silicic magmatic system: insights from mineral diffusive profiles in the Kidnappers and Rocky Hill deposits, New Zealand. Earth Planet. Sci. Lett. 473, 1–13. https://doi.org/10.1016/j.epsl.2017.05.036.

Cunningham, H.S., Turner, S.P., Patia, H., Wysoczanski, R., Nichols, A.R.L., Eggins, S., Dosseto, A., 2009. (^{210}Pb/^{226}Ra) variations during the 1994–2001 intracaldera volcanism at Rabaul Caldera. J. Volcanol. Geotherm. Res. 184, 416–426. https://doi.org/10.1016/j.jvolgeores.2009.04.018.

Druitt, T.H., Edwards, L., Mellors, R.M., Pyle, D.M., Sparks, R.S.J., Lanphere, M., Davies, M., Barriero, B., 1999. Santorini Volcano. Geological Society Memoir. Geological Society, London.

Druitt, T.H., Costa, F., Deloule, E., Dungan, M., Scaillet, B., 2012. Decadal to monthly timescales of magma transfer and reservoir growth at a caldera volcano. Nature 482, 77–80. https://doi.org/10.1038/nature10706.

Dufek, J., Bachmann, O., 2010. Quantum magmatism: magmatic compositional gaps generated by melt-crystal dynamics. Geology 38, 687–690. https://doi.org/10.1130/G30831.1.

Fabbro, G.N., Druitt, T.H., Scaillet, S., 2013. Evolution of the crustal magma plumbing system during the build-up to the 22-ka caldera-forming eruption of Santorini (Greece). Bull. Volcanol. 75, 1–22. https://doi.org/10.1007/s00445-013-0767-5.

Fabbro, G.N., Druitt, T.H., Costa, F., 2017. Storage and eruption of silicic magma across the transition from dominantly effusive to caldera-forming states at an arc volcano (Santorini, Greece). J. Petrol. 58, 2429–2464. https://doi.org/10.1093/petrology/egy013.

Finney, B., Turner, S., Hawkesworth, C., Larsen, J., Nye, C., George, R., Bindeman, I., Eichelberger, J., 2008. Magmatic differentiation at an island-arc caldera: Okmok Volcano, Aleutian Islands, Alaska. J. Petrol. 49, 857–884. https://doi.org/10.1093/petrology/egn008.

Fisher, N., 1939. Geology and vulcanology of Blanche Bay, and the surrounding area, New Britain. Territory N. G. Geol. Bull. 1, 68.

Giordano, D., Russell, J.K., Dingwell, D.B., 2008. Viscosity of magmatic liquids: a model. Earth Planet. Sci. Lett. 271, 123–134. https://doi.org/10.1016/j.epsl.2008.03.038.

Global Volcanism Program, 1994. Report on Rabaul (Papua New Guinea). Bull. Glob. Volc. Netw. 19. https://doi.org/10.5479/si.GVP.BGVN199408-252140.

Global Volcanism Program, 2006. Report on Rabaul (Papua New Guinea). Bull. Glob. Volc. Netw., 31 https://doi.org/10.5479/si.GVP.BGVN200609-252140.

Global Volcanism Program, 2014. Report on Rabaul (Papua New Guinea). Bull. Glob. Volc. Netw., 39 https://doi.org/10.5479/si.GVP.BGVN201408-252140.

Hawkesworth, J., Byron, J., Wallis, S., Carteret, P., Cook, J., Banks, J., 1773. An account of the voyages undertaken by the order of His present Majesty for making discoveries in the Southern Hemisphere, and successively performed by Commodore Byron, Captain Wallis, Captain Carteret, and Captain Cook. The Dolphin, the Swallow, and the Endeavour: Drawn Up From the Journals Which Were Kept by the Several Commanders, and From the Papers of Joseph Banks, Esq, Second edition W. Strahan and T. Cadell, London.

Heming, R.F., 1974. Geology and petrology of Rabaul Caldera, Papua New Guinea. Geol. Soc. Am. Bull. 85, 1253–1264. https://doi.org/10.1130/0016-7606(1974)85<1253:GAPORC>2.0.CO;2.

Heming, R.F., 1977. Mineralogy and proposed P–T paths of basaltic lavas from Rabaul caldera, Papua New Guinea. Contrib. Mineral. Petrol. 61, 15–33. https://doi.org/10.1007/BF00375943.

Heming, R.F., Carmichael, I.S.E., 1973. High-temperature pumice flows from the Rabaul caldera Papua, New Guinea. Contrib. Mineral. Petrol. 38, 1–20. https://doi.org/10.1007/BF00371723.

Holm, R.J., Rosenbaum, G., Richards, S.W., 2016. Post 8 Ma reconstruction of Papua New Guinea and Solomon Islands: microplate tectonics in a convergent plate boundary setting. Earth Sci. Rev. 156, 66–81. https://doi.org/10.1016/j.earscirev.2016.03.005.

Johnson, R.W., Threlfall, N.A., 1985. Volcano Town: The 1937–43 Rabaul Eruptions. Robert Brown & Associates, Bathurst, NSW, Australia.

Johnson, R.W., Everingham, I.B., Cooke, R.J.S., 1981. Submarine volcanic eruptions in Papua New Guinea: 1878 activity of Vulcan (Rabaul) and other examples. Geological Survey of Papua New Guinea Memoir, Volume of Volcanological Papers 10, pp. 167–179.

Johnson, R.W., Itikarai, I., Patia, H., McKee, C.O., 2010. Volcanic Systems of the Northeastern Gazelle Peninsula, Papua New Guinea: Synopsis, Evaluation, and a Model for Rabaul Volcano. Rabaul Volcano Workshop Report. Papua New Guinea Department of Mineral Policy and Geohazards Management and Australian Agency for International Development, Port Moresby, Papua New Guinea.

Karlstrom, L., Wright, H.M., Bacon, C.R., 2015. The effect of pressurized magma chamber growth on melt migration and pre-caldera vent locations through time at Mount Mazama, Crater Lake, Oregon. Earth Planet. Sci. Lett. 412, 209–219. https://doi.org/10.1016/j.epsl.2014.12.001.

McKee, C.O., 2015. Tavui Volcano: neighbour of Rabaul and likely source of the Middle Holocene penultimate major eruption in the Rabaul area. Bull. Volcanol. 77, 1–21. https://doi.org/10.1007/s00445-015-0968-1.

McKee, C.O., Duncan, R.A., 2016. Early volcanic history of the Rabaul area. Bull. Volcanol. 78, 1–28. https://doi.org/10.1007/s00445-016-1018-3.

McKee, C.O., Fabbro, G.N., 2018. The Talili Pyroclastics eruption sequence: VEI 5 precursor to the seventh century CE caldera-forming event at Rabaul, Papua New Guinea. Bull. Volcanol. 80, 79. https://doi.org/10.1007/s00445-018-1255-8.

McKee, C.O., Mori, J., Talai, B., 1989. Microgravity changes and ground deformation at Rabaul Caldera, 1973–1985. In: Latter, J.H. (Ed.), Volcanic Hazards, IAVCEI Proceedings in Volcanology. Springer, Berlin Heidelberg, pp. 399–428. https://doi.org/10.1007/978-3-642-73759-6_24.

McKee, C.O., Baillie, M.G., Reimer, P.J., 2015. A revised age of AD 667–699 for the latest major eruption at Rabaul. Bull. Volcanol. 77, 65. https://doi.org/10.1007/s00445-015-0954-7.

McKee, C.O., Kuduon, J., Patia, H., 2016. Recent eruption history at Rabaul: volcanism since the 7th century AD caldera-forming eruption. Geohazards Management Division Report 2016/01.

McKee, C.O., Itikarai, I., Kuduon, J., Lauer, N., Lolok, D., Patia, H., de Saint Ours, P., Saunders, S.J., Sipison, L., Stewart, R., Talai, B., Taranu, F., Davies, H.L., 2018. The 1994–1998 eruptions at Rabaul: main features and analysis. Geohazards Management Division Report 2018/02.

Mori, J., McKee, C., Itikarai, I., Lowenstein, P., de Saint Ours, P., Talai, B., 1989. Earthquakes of the Rabaul seismo-deformational crisis September 1983 to July 1985: seismicity on a caldera ring fault. In: Latter, J.H. (Ed.), Volcanic Hazards, IAVCEI Proceedings in Volcanology. Springer, Berlin Heidelberg, pp. 429–462. https://doi.org/10.1007/978-3-642-73759-6_25.

Nairn, I.A., Talai, B., Wood, C.P., McKee, C.O., 1989. Rabaul Caldera, Papua New Guinea—1:25,000 Reconnaissance Geological Map and Eruption History.

Nairn, I.A., McKee, C.O., Talai, B., Wood, C.P., 1995. Geology and eruptive history of the Rabaul Caldera area, Papua New Guinea. J. Volcanol. Geotherm. Res. 69, 255–284. https://doi.org/10.1016/0377-0273(95)00035-6.

Pansino, S., Taisne, B., 2019. How magmatic storage regions attract and repel propagating dikes. J. Geophys. Res. Solid Earth 124, 274–290. https://doi.org/10.1029/2018JB016311.

Papike, J.J., Cameron, K.L., Baldwin, K., 1974. Amphiboles and pyroxenes: characterization of other than quadrilateral components estimates of ferric iron from microprobe data. Geol. Soc. Am. Abstr. Programs 6, 1053–1054.

Patia, H., 2004. Petrology and Geochemistry of the Recent Eruption History at Rabaul Caldera, Papua New Guinea: Implications for Magmatic Processes and Recurring Volcanic Activity (M. Phil). Australian National University, Canberra.

Patia, H., Eggins, S.M., Arculus, R.J., McKee, C.O., Johnson, R.W., Bradney, A., 2017. The 1994–2001 eruptive period at Rabaul, Papua New Guinea: petrological and geochemical evidence for basalt injections into a shallow dacite magma reservoir, and significant SO_2 flux. J. Volcanol. Geotherm. Res. 345, 200–217. https://doi.org/10.1016/j.jvolgeores.2017.08.011.

Pinel, V., Jaupart, C., 2000. The effect of edifice load on magma ascent beneath a volcano. Philos. Trans. R. Soc. London, Ser. A 358, 1515–1532. https://doi.org/10.1098/rsta.2000.0601.

Putirka, K.D., 2008. Thermometers and barometers for volcanic systems. Rev. Mineral. Geochem. 69, 61–120. https://doi.org/10.2138/rmg.2008.69.3.

Roggensack, K., Williams, S.N., Schaefer, S.J., Parnell, R.A., 1996. Volatiles from the 1994 eruptions of Rabaul: understanding large caldera systems. Science 273, 490–493. https://doi.org/10.1126/science.273.5274.490.

Shane, P., 2015. Contrasting plagioclase textures and geochemistry in response to magma dynamics in an intra-caldera rhyolite system, Okataina volcano. J. Volcanol. Geotherm. Res. 297, 1–10. https://doi.org/10.1016/j.jvolgeores.2015.03.013.

Sparks, R.S.J., Marshall, L.A., 1986. Thermal and mechanical constraints on mixing between mafic and silicic magmas. J. Volcanol. Geotherm. Res. 29, 99–124. https://doi.org/10.1016/0377-0273(86)90041-7.

Vigneresse, J.L., Barbey, P., Cuney, M., 1996. Rheological transitions during partial melting and crystallization with application to felsic magma segregation and transfer. J. Petrol. 37, 1579–1600. https://doi.org/10.1093/petrology/37.6.1579.

Walker, G.P.L., 1983. Ignimbrite types and ignimbrite problems. J. Volc. Geotherm. Res. Explosive Volc. 17, 65–88. https://doi.org/10.1016/0377-0273(83)90062-8.

Walker, G.P.L., Heming, R.F., Sprod, T.J., Walker, H.R., 1981. Latest major eruptions of Rabaul volcano. Geological Survey of Papua New Guinea Memoir, Volume of Volcanological Papers 10, pp. 181–193.

Wood, C.P., Nairn, I.A., McKee, C.O., Talai, B., 1995. Petrology of the Rabaul Caldera area, Papua New Guinea. J. Volcanol. Geotherm. Res. 69, 285–302. https://doi.org/10.1016/0377-0273(95)00034-8.